An Inline Compact SIW Bandpass Filter With Quasi-Elliptic Response Using Microstrip Extracted-Pole Resonators

Yilong Zhu, *Member, IEEE*, Yuandan Dong, *Senior Member, IEEE*, Jens Bornemann, *Life Fellow, IEEE*, Lin Gu, *Student Member, IEEE*, and Deisy Formiga Mamedes, *Member, IEEE*

***Abstract*—Two novel types of microstrip-based extracted-pole resonators are investigated in this brief, which are able to achieve a one-pole response with a transmission zero (TZ) created either below or above the passband. Resonance and transfer characteristics of the resonators are studied and discussed. And a detailed analysis is demonstrated by theoretical derivation and simulation. The application of the proposed extracted-pole resonators to an inline quasi-elliptic substrate integrated waveguide (SIW) filter is then presented, which exhibits a compact size and high selectivity with a TZ located on both sides of the passband. To verify the proposed concept, a filter prototype with a center frequency of 10 GHz is designed and fabricated. And the measured results show good agreement with the simulation, presenting a quasi-elliptic response with high selectivity.**

***Index Terms*—Compact size, extracted-pole resonators, quasi-elliptic response, inline filter, substrate integrated waveguide.**

I. Introduction

As a typical application of substrate integrated wave guide (SIW) technology, bandpass filters, especially for quasi-elliptic filters [1], [2], are required to have sharp skirts with transmission zeros (TZs) at both sides of passbands. A widely used approach to produce TZs is to construct cross couplings between non-adjacent cavities, which can be achieved in three ways, including: 1) Using overmoded cavities whose dominant modes are used to operate cross couplings [3], [4]; 2) Establishing multipath coupling diagrams on a multilayer SIW configuration [5]; and 3) Constructing negative-coupling structures [6], [7], [8]. The third method is most widely used among them, but it also brings drawbacks such as structural complexity and degraded unloaded quality factors, and a triplet/quadruplet filter topology is also inevitable in order to implement negative-coupling structures. In addition to utilizing cross couplings, other methods such as using mixed electric and magnetic couplings [9] and bandpass-bandstop filter cascades [10], [11] are also popular to create TZs. The former method is able to create a TZ in the lower (or upper) stopband when the mixed coupling is capacitively (or inductively) dominant. The latter provides a simple and new method to dynamically tune the TZs, but it would significantly increase filter size.

In addition to using the above methods, another way known as extracted-pole technique has also been proposed [12], [13], which shows the merit to create TZs in an inline filter configuration. This technique has been widely employed in waveguide [14] and microstrip structures [15]. When applying it to SIW platform, some realizable applications of quasi-elliptic filters have been reported. For example, an SIW filter with two extracted-pole SIW cavities loaded at the source and load has been proposed to achieve a 4-pole quasi-elliptic response in [16], but the filter size is overwhelming due to the indispensable waveguide sections. Utilizing microstrip stubs as extracted-pole units, half-mode SIW filters with TZs created above the passband are presented in [17], [18]. However, they only achieve TZs placed at the right side of the passband.

In this brief, two novel extracted-pole resonators are investigated. The first one presents a one-pole response with a T created above the passband, while the TZ is produced below the passband for the second one. By applying these resonators to SIW cavities, an inline quasi-elliptic filter operated at X-band is then studied and implemented, which exhibits high selectivity with a TZ located at both sides of the passband. It presents some special merits, including: 1) compared with conventional SIW filters, the proposed filter shows a compact size while maintaining a moderate unloaded quality factor of 285; and 2) by loading the extracted-pole resonators at two sides of SIW cavities, an inline quasi-elliptic filter with high selectivity can be simply realized without negative-coupling structures.

II. Two Types of Extracted-Pole Resonators

A. Proposed Resonators and Their Equivalent Circuits

Fig. 1 shows the layouts of the proposed extracted-pole resonators and their equivalent circuits, which are able to generate a T below or above the passband, respectively.

As shown in Fig. 1(a), the first resonator is composed of a circular patch and a uniform impedance micro strip stub.

Manuscript received 9 November 2022; revised 18 December 2022; accepted 20 December 2022. Date of publication 22 December 2022; date of current version 8 June 2023. This work was supported by the Natural Sciences and Engineering Research Council (NSERC) of Canada. The work of Yilong Zhu was supported by the China Scholarship Council (CSC) under Grant 202006070154. This brief was recommended by Associate Editor M. Yavari. *(Corresponding author: Yuandan Dong.)*

Yilong Zhu is with the School of Electronic Science and Engineering, University of Electronic Science and Technology of China, Chengdu 611731, China, and also with the Department of Electrical and Computer Engineering, University of Victoria, Victoria, BC V8W 2Y2, Canada.

Yuandan Dong and Lin Gu are with the School of Electronic Science and Engineering, University of Electronic Science and Technology of China, Chengdu 611731, China (e-mail: ydong@uestc.edu.cn).

Jens Bornemann and Deisy Formiga Mamedes are with the Department of Electrical and Computer Engineering, University of Victoria, Victoria, BC V8W 2Y2, Canada (e-mail: j.bornemann@ieee.org; mamedes@ieee.org).

Color versions of one or more figures in this article are available at https://doi.org/10.1109/TCSII.2022.3231577.

Digital Object Identifier 10.1109/TCSII.2022.3231577

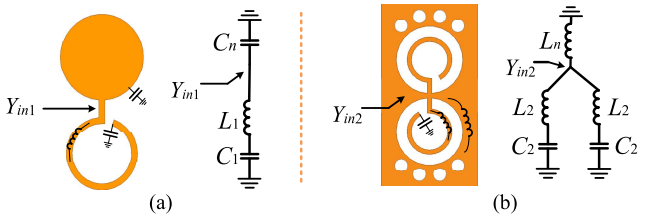

Fig. 1. (a) First extracted-pole resonator and its equivalent circuit. (b) Second extracted-pole resonator and its equivalent circuit.

Seen from the center of the resonator, the circular patch can be considered as a capacitor (C_n) due to the existing capacitance between the patch and ground, while the microstrip stub can be considered as a resonant circuit consisting of an inductor (L_1) in series with a capacitor (C_1).

As for the second extracted-pole resonator in Fig. 1(b), it is first reported in our previous paper [19], but a theoretical investigation in terms of its electrical performance is still missing. It is composed of two circular uniform impedance micro strip stubs, which are of the same size and rotationally symmetric surrounded by the two metallic-via arrays. Seen from the center of the resonator, each of the circular stubs is equivalent to an inductor (L_2) in series with a capacitor (C_2), while the other parts can be regarded as an inductor (L_n) due to the metallic vias as depicted in Fig. 1(b).

B. Theoretical Analysis

The first extracted-pole resonator is equivalent to an *LC* resonant circuit as shown in Fig. 1(a), and its input admittance can be derived as follows

$$Y_{in1} = j\omega\left(\frac{C_1 + C_n - \omega^2 L_1 C_1 C_n}{1 - \omega^2 L_1 C_1}\right) \tag{1}$$

where ω represents the angular frequency. The resonance (ω_{p1}) of the resonator occurs at the frequency where the imaginary part of Y_{in1} equals zero (*i.e.*, $Im(Y_{in1}) = 0$). It can be obtained by

$$\omega_{p1} = \sqrt{\frac{1}{L_1 C_1} + \frac{1}{L_1 C_1}} \tag{2}$$

In addition, a transmission zero would be generated if the imaginary part of Y_{in1} goes to infinity. Herein, if we let the denominator of (1) vanish, then the transmission zero occurs at

$$\omega_{z1} = \sqrt{\frac{1}{L_1 C_1}} \tag{3}$$

Comparing (2) with (3), it shows that ω_{z1} is always less than ω_{p1}, indicating that a TZ is created below the passband for the first extracted-pole resonator. For validation, the electromagnetic- (EM-) and circuit-based transfer responses are performed in Fig. 2, in which the corresponding circuit and EM models are also inset. As depicted, the simulated center frequencies are set at 10 GHz with a TZ occurring at 9.18 GHz in the lower stopband. This result shows good agreement with the theoretical analysis that a TZ is always created below the passband.

Similarly, the second resonator is equivalent to the *LC* resonant circuit shown in Fig. 1(b), and its input admittance can be derived as

$$Y_{in2} = -j\frac{1 - \omega^2 C_2(L_2 + 2L_2)}{(1 - \omega^2 L_2 C_2)(\omega L_n)} \tag{4}$$

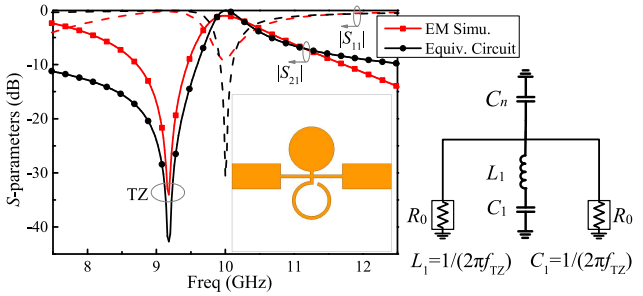

Fig. 2. Transfer responses of the first extracted-pole resonator with EM model and its equivalent circuit (L_1 = 17.34 pH, C_1 = 17.34 pf; C_n = 92.88 pF).

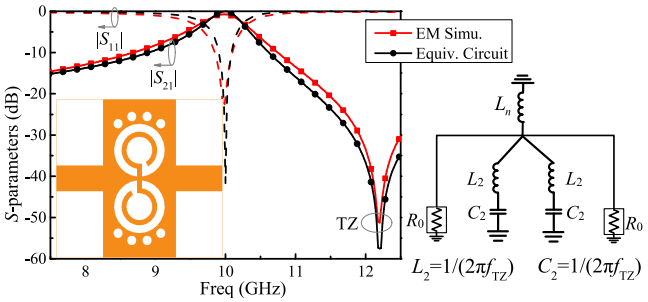

Fig. 3. Transfer responses of the second extracted-pole resonator with EM model and its equivalent circuit (L_2 = 13.05 pH, C_2 = 13.05 pf, L_n = 3.18 pH).

If we let the imaginary part of Y_{in2} approaches zero and infinity, then the resonant frequency (ω_{p2}) and transmission zero (ω_{z2}) can be obtained as

$$\omega_{p2} = \frac{1}{\sqrt{(L_2 + 2L_n)C_2}} \tag{5}$$

$$\omega_{z2} = \sqrt{\frac{1}{L_2 C_2}} \tag{6}$$

In comparison with the first resonator, the second one shows reversed zero-pole characteristics. From (5) and (6), it follows that the frequency of the transmission zero (ω_{z2}) is always greater than that of the transmission pole (ω_{p2}), indicating that a TZ is produced above the passband for the second extracted-pole resonator. To validate this, EM- and circuit-based transfer responses are simulated as presented in Fig. 3, whose passband centers are set at 10 GHz. It can be observed that a TZ appears at 12.2 GHz in the upper stopband, verifying the theoretical analysis that a TZ always occurs above the passband for the second resonator.

C. Resonance and Transfer Characteristics

To further explore the resonators' transfer and resonance characteristics, such as control of bandwidth, adjustment of transmission poles and zeros, etc., Figs. 4 and 5 present circuit- simulated *S*-parameters versus some key circuit elements, including frequencies of the transmission zero, capacitance C_n and inductance L_n.

For the first resonator, Fig. 4(a) presents the simulated *S*-parameters versus variable frequency of the T, which is placed at 7 GHz, 8 GHz and 9 GHz, respectively. When the TZ's frequency increases, the transmission pole (TP) also moves towards higher frequencies, while the bandwidth slightly reduces in this process. Fig. 4(b) shows the simulated *S*-parameters versus variable capacitance C_n with the TZ fixed

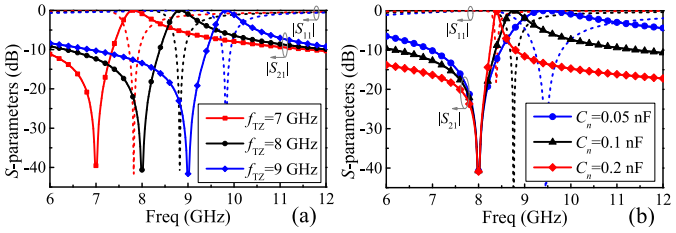

Fig. 4. Circuit-simulated S-parameters of the first resonator versus (a) variable frequency of the TZ, and (b) variable capacitance C_{n}.

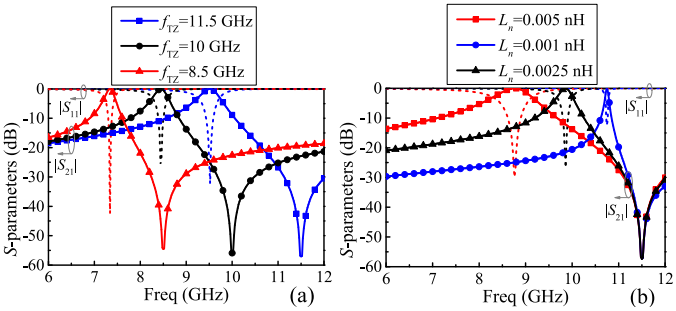

Fig. 5. Circuit-simulated S-parameters of the second resonator versus (a) variable frequency of the TZ, and (b) variable inductance L_{n}.

at 8 GHz. It is observed that the resonant frequency increases with the decrease of C_{n}, and the bandwidth is significantly enlarged as well.

Similarly, the corresponding simulations are also performed for the second resonator. Fig. 5(a) shows the simulated S-parameters versus variable frequency of the TZ, which is located at 8.5 GHz, 10 GHz and 11.5 GHz, respectively. As the TZ moves to higher frequencies, the TP also moves with slightly increased bandwidth. To investigate the impact of the inductance L_{n}, Fig. 5(b) presents the simulated S-parameters versus L_{n} with the TZ fixed at 11.5 GHz. It is seen that the resonant frequency increases with the decrease of L_{n}, accompanied by a significantly decreased bandwidth.

Although the proposed extracted-pole resonators present different zero-pole features, the above simulations indicate they also embrace some similar electrical performance, including: 1) if the TZ is moved, the TP would be significantly affected as well, meanwhile the bandwidth is only slightly changed; and 2) for the two resonators, when the frequencies of the TZ and TP are close to each other, the bandwidth becomes narrower. But if their frequencies are far apart from each other, the bandwidth is enlarged. These features provide a technical guideline for filter design, especially for the adjustment of TZs, TPs and bandwidths of filters. For example, by utilizing the two resonators, a wideband filter can be realized when the TZs are placed far away from the passband, while the TZs have to get close to the passband to perform a narrowband filter.

III. In-Line Quasi-Elliptic SOW Filter Design

A. Coupling Topology and Operation

The topology of the two proposed resonators can be regarded as an extracted-pole section [13], which is composed of a non-resonant node connecting to a resonant node as shown in Fig. 6. For filter applications, as depicted in Fig. 6(a), the simplest coupling topology is to cascade the two extracted-pole sections to form a two-pole filter, which therefore is able

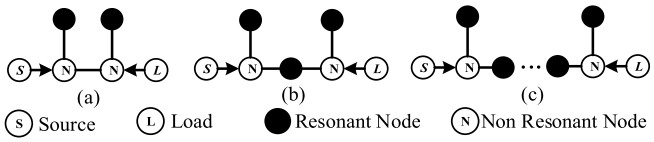

Fig. 6. Coupling typologies of the (a) 2nd-order, (b) 3rd-order and (c) expanded n^{th}-order extracted-pole filters.

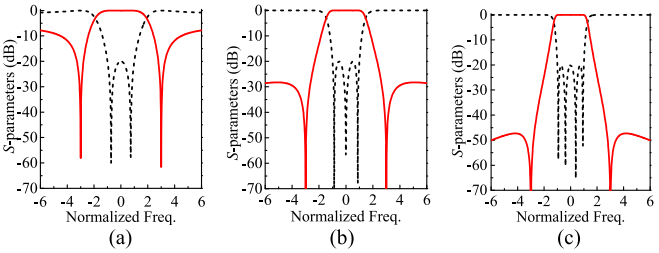

Fig. 7. Normalized S-parameters of (a) 2nd-order, (b) 3rd-order and (c) 4th-order extracted-pole filters with two TZs placed at $\pm 3j$ (S_{11} – dashed, S_{21} – solid line).

to produce a TZ at both sides of the passband. However, low-order filters are usually unable to present outstanding electrical performance such as high selectivity and sufficient out-of-band rejection. To extend the filter's order, extra resonant nodes can be simply inserted between the two extracted-pole sections. Shown in Fig. 6(b), a 3rd-order filter topology can be performed by inserting a traditional resonant node. In addition, as presented in Fig. 6(c), this method can also be further extended to achieve an n^{th}-order filter by inserting $n-2$ resonant nodes between the two extracted-pole sections. All these topologies are able to formulate quasi-elliptic filtering responses, which have a TZ located at each side of the passbands.

To demonstrate the above coupling typologies, Fig. 7 shows three illustrative prototypes corresponding to the topologies in Fig. 6, which present normalized 2-, 3- and 4-pole responses, respectively. All their TZs are placed at $\pm 3j$. Shown in Fig. 7(a), the two extracted-pole sections can create two transmission poles as well as a TZ located at each side of the passband. By inserting extra resonant nodes, higher order filtering responses can be achieved with improved selectivity and out-of-band rejection as depicted in Figs. 7(b) and 7(c). For practical realizations, a tradeoff between insertion loss (IL) and the filter order should be taken into consideration due to the finite unloaded quality factors of the resonators.

On the other hand, other topological forms, such as placing multiple TZs at each (or only one) side of the passband, are also realizable. A reasonable combination of the proposed extracted-pole sections can be considered for this purpose.

B. Filter Design and Analysis

By utilizing the two extracted-pole resonators, a 4th-order inline quasi-elliptic filter is proposed for demonstration. Fig. 8 shows the layout of the proposed filter, in which two SOW cavities are inserted between the two extracted-pole sections. Theoretically, the filter would generate a 4-pole quasi-elliptic response with a TZ located at each side of the passband. Compared with full-mode quasi-elliptic SIW filters whose TZs are produced by the negative-coupling structures [6], [7], [8], the proposed filter shows merits of a compact size and an inline configuration without applications of negative couplings.

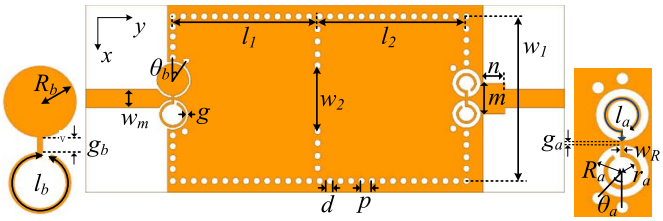

Fig. 8. Layout of the proposed inline quasi-elliptical SOW filter. (Initial dimensions in mm: $l_1 = 13.3$, $l_2 = 13.68$, $w_1 = 15.29$, $w_2 = 6.05$, g = 0.2, $w_m = 1.57$, $m = 3$, $n = 2$, $d = 0.6$, $p < 1$, $w_R = 0.2$, $l_a = 5.276$, $\theta_a = 41.5^o$, $R_a = 1.329$, $r_a = 0.729$, $g_a = 0.2$, $\theta_b = 35^o$, $R_b = 1.47$, $l_b = 6.676$, $g_b = 0.5$.

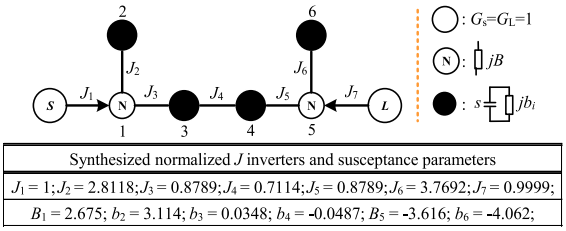

Synthesized normalized J inverters and susceptance parameters
$J_1 = 1; J_2 = 2.8118; J_3 = 0.8789; J_4 = 0.7114; J_5 = 0.8789; J_6 = 3.7692; J_7 = 0.9999;$
$B_1 = 2.675; b_2 = 3.114; b_3 = 0.0348; b_4 = -0.0487; B_5 = -3.616; b_6 = -4.062;$

Fig. 9. Coupling schematic topology and its synthesized normalized J inverters and acceptance parameters of the proposed filter.

The coupling topology of the filter can be depicted as shown in Fig. 9, in which the non-resonant nodes are represented by constant acceptance jB and the resonant nodes are considered as a unit capacitor in parallel with constant susceptance jb_i. For demonstration, the proposed filter is synthesized with a 4th-order quasi-elliptic response, whose center frequency is set at 10 GHz with an in-band return loss of 20 dB and an equal-ripple bandwidth of 0.89 GHz (corresponding to a 3-dB bandwidth of 1.13 GHz). The finite TZs are pre-defined at $f_1 = 8.7$ GHz and $f_2 = 12$ GHz, corresponding to normalized frequencies of $\Omega_1 = -3.114$ and $\Omega_2 = 4.062$, respectively. According to the synthesis method in [13], the synthesized elements can be determined as presented in Fig. 9, in which normalized J inverters and susceptance parameters are obtained. With these synthesized parameters, the initial dimensions can be determined in practical filter implementation. The J inverters between the adjacent resonant sections (J_3, J_4 and J_5) can be controlled, respectively, by parameters θ_b, w_2 and θ_a (c.f. Fig. 8).

IV. Fabrication, Measurements, and Discussion

A. Fabrication and Experiments

The proposed filter is implemented on 0.508mm-thickness RT/During 5880 substrate. Fig. 10(a) shows the fabricated filter prototype, which presents an overall circuit size of 20.4 mm × 37.9 mm ($1.18\lambda_g \times 0.57\lambda_g$). As shown in Fig. 10(b), the measurements were carried out on an Anritsu 3680 test fixture with thru-reflect-line (TRL) calibration.

Fig. 11 depicts the synthesized, simulated and measured S-parameters with narrow band and broadband intervals, which show quasi-elliptic responses in good agreement. It is expected that the TZs occur at each side of the passband, exhibiting high selectivity and improved out-of-band rejection. The measured center frequency is 9.99 GHz, which slightly deviates downwards from that of the simulation. The measured minimal IL is 0.87 dB with a 3-dB bandwidth of 1.06 GHz, compared to the simulated minimal IL of 0.83 dB with a 3-dB bandwidth of 1.09 GHz. As for the measured return loss, it is greater than 13.1 dB within the passband. Slight discrepancies between simulated and measured return loss were to be

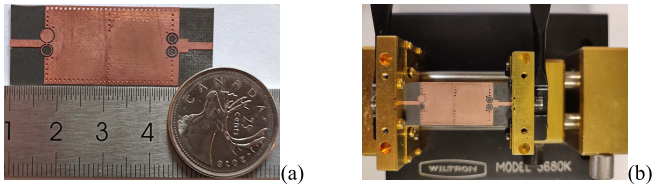

Fig. 10. (a) Photograph of the fabricated inline extracted-pole filter. (b) Photograph of the measurement setup with an Pantsuit 3680 test fixture.

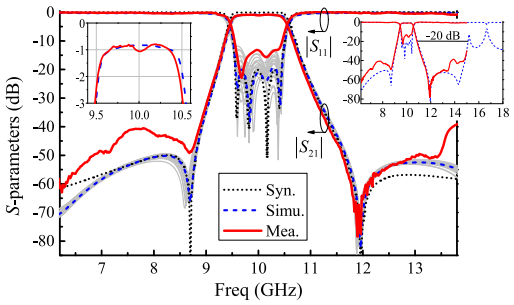

Fig. 11. Synthesized, measured and simulated S-parameters of the proposed filter and its tolerance analysis against some key dimensional parameters.

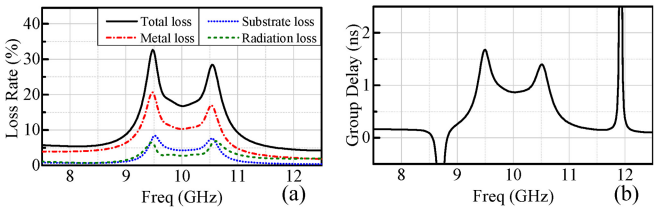

Fig. 12. (a) Simulated radiation, substrate, metal and total losses (calculated by the formula $R = 1\text{-}|S_{11}|^2\text{-}|S_{21}|^2$). (b) Simulated group delay of the proposed filter.

expected due to the fabrication tolerance. A robustness analysis against this kind of tolerance is performed in Fig. 11, which is obtained by minorly varying some dimensions of the two extracted-pole resonators. It is seen that the return loss shows a notable fluctuation with regard to dimensional variations, while other features such as center frequency and bandwidth almost maintain stable.

B. Dissipation and Unloaded Quality Factor

To study the dissipation effects of the proposed filter, three main loss factors, including radiation, finite metal conductivity and dielectric loss are investigated. By running the simulations of setting the metal and substrate layers lossless, Fig. 12(a) depicts the energy loss rates caused by these factors. It is seen that the metal loss is the dominant contribution to the energy dissipation, while radiation and substrate losses are relatively low. To investigate the average unloaded quality factor (Q_u) of the filter, the simulated group delay is depicted in Fig. 12(b) and it is 0.868 NS at the band center. By assuming that the proposed filter is uniform-Q_u, its average Q_u can be associated with insertion losses (A_0) and group delays (τ_{BPF}) using (7) [20]

$$A_0 \approx 20 \log e \cdot \frac{\Delta\omega \cdot \tau_{BPF}}{2FBW \cdot Q_u} \tag{7}$$

Since the simulated insertion loss at the band center is 0.83 dB, the average Q_u is calculated as 285. Meanwhile, the two extracted-pole resonators and the SOW cavities show

TABLE I
COMPARISON OF STATE-OF-THE-ART SI FILTERS

	Technology	layer	Order	f_c (GHz)	IL (dB)	3-dB FBW (%)	Q_u	No. of TZs	Ways to create TZs	Circuit Size ($\lambda_g \times \lambda_g$)
[4]-I	SIW	Single	4	10	1.78	4.2	N/A	2	Bypass coupling	0.95 × 1.35
[5]	air-filled SIW	Triple	4	20.99	0.71	1.66	1478	2	Cross couplings	1.02 × 1.11
[6]	SIW	Single	6	12.6	1.4	10	260	2	Cross couplings	N/A
[7]-I	SIW	Single	4	20.5	0.9	3.9	500	2	Cross couplings	0.93×0.97
[8]	Combline SIW	Single	4	5.75	3.6	2.0	225	2	Cross couplings	0.86 × 0.86
[16]	SIW	Single	4	9.82	3	*2	N/A	2	Extracted-pole sections	2.34×0.91
[17]-I	HMSIW & Microstrip	Single	2	6.6	<1	N/A	N/A	2	Extracted-pole sections	N/A
[18]	HMSIW & Microstrip	Single	3	4.45	1.95	7.8	130	1	Extracted-pole sections	1.30 × 0.65
This Work	SIW & Microstrip	Single	4	9.99	0.87	10.9	285	2	Extracted-pole sections	1.18 × 0.57

*: equal-ripple bandwidth, N/A: not applicable.

Q_u values of 264, 229, and 435 using the eigenmode simulations in the numerical tool, respectively, which indicates that the hybrid-structure filter shows a moderate Q_u between the microstrip extracted-pole resonators and the SIW cavities.

C. Comparison and Discussion

Table I presents a performance comparison of the proposed filter with other SOW filters. It has been the most popular way to create TZs by using cross couplings [5], [6], [8], but folded filter configurations are unavoidable in order to construct negative-coupling structures. Utilizing the extracted-pole technique, an inline SIW filter with a TZ produced at each side of the passband is realized in [16], but it leads to gigantic filter size due to the oversized extracted-pole sections. To reduce volume, the microstrip extracted-pole resonators are applied on a half-mode SIW (HMSIW) platform in [17] and [18]. However, the TZs can only be created above the passbands, and it also leads to declined Q_u values using the HMSIW cavities. In this brief, two novel extracted-pole resonators, which show different zero-pole characteristics, are studied to design a quasi-elliptic SIW filter. It shows merits of generating a TZ at both sides of the passband in an inline filter configuration. In addition, compared with the full-mode SIW filters in [4], [7] and [16], the proposed filter shows a compact size with a moderate Q_u.

V. CONCLUSION

Two novel extracted-pole resonators are presented and studied in this brief, whose resonance characteristics are well discussed by theoretical derivation and simulation. To illustrate their applications, an inline quasi-elliptic SOW filter is proposed, which presents high selectivity with a TZ created at each side of the passband. In addition, a compact size and a moderate Q_u are also realized due to the hybrid microstrip-SIW structure. The proposed extracted-pole resonators, which present one-pole responses with a natural TZ, can be considered as a feasible technique to achieve quasi-elliptic filter on a SIW platform, especially for inline filter configuration. This kind of filters are very suitable to be integrated in PCB circuits for base station communication applications.

REFERENCES

[1] L. Gu and Y. Dong, "A compact, hybrid SIW filter with controllable transmission zeros and high selectivity," *IEEE Trans. Circuits Syst. II, Exp. Briefs*, vol. 69, no. 4, pp. 2051–2055, Apr. 2022.

[2] Y. Zhu and Y. Dong, "A compact dual-band quasi-elliptic filter based on hybrid SIW and microstrip technologies," *IEEE Trans. Circuits Syst. II, Exp. Briefs*, vol. 69, no. 3, pp. 719–723, Mar. 2022.

[3] S. Amari and U. Rosenberg, "Characteristics of cross (bypass) coupling through higher/lower order modes and their applications in elliptic filter design," *IEEE Trans. Microw. Theory Techn.*, vol. 53, no. 10, pp. 3135–3141, Oct. 2005.

[4] Q. Liu, D. Zhou, and D. Zhang, "SIW bandpass filters in modified box-section scheme with bypass/constant/frequency dependent coupling in diagonal cross-coupling path," *IET Microw. Antennas Propag.*, vol. 13, no. 5, pp. 559–566, Apr. 2019.

[5] T. Martin, A. Ghiotto, T.-P. Vuong, K. Wu, and F. Lotz, "Compact quasi-elliptic and highly selective AFSIW filter with multilayer cross-coupling," in *IEEE MTT-S Int. Microw. Symp. Dig.*, Boston, MA, USA, Jun. 2019, pp. 718–721.

[6] D. L. Diedhiou, E. Rius, J.-F. Favennec, and A. El Mostrah, "Ku-band cross-coupled ceramic SIW filter using a novel electric cross-coupling," *IEEE Microw. Wireless Compon. Lett.*, vol. 25, no. 2, pp. 109–111, Feb. 2015.

[7] X. Chen and K. Wu, "Substrate integrated waveguide cross-coupled filter with negative coupling structure," *IEEE Trans. Microw. Theory Techn.*, vol. 56, no. 1, pp. 142–149, Jan. 2008.

[8] S. Sirci, F. Gentili, J. D. Martínez, V. E. Boria, and R. Sorrentino, "Quasi-elliptic filter based on SIW combline resonators using a coplanar line cross-coupling," in *IEEE MTT-S Int. Microw. Symp. Dig.*, Phoenix, AZ, USA, May 2015, pp. 1–4.

[9] Q. Liu, D. Zhang, D.-F. Zhou, Y. Liu, and D. Lv, "Inline asymmetric response quarter-mode SIW bandpass filters with controllable mixed electric and magnetic coupling," in *Proc. Int. Symp. Antennas Propag. (ISAP)*, Xi'an, China, 2019, pp. 1–3.

[10] E. J. Naglich, J. Lee, D. Peroulis, and W. J. Chappell, "Bandpass–bandstop filter cascade performance over wide frequency tuning ranges," *IEEE Trans. Microw. Theory Techn.*, vol. 58, no. 12, pp. 3945–3953, Dec. 2010.

[11] S. Saeedi, J. Lee, and H. H. Sigmarsson, "Tunable, high-Q, substrate-integrated, evanescent-mode cavity bandpass-bandstop filter cascade," *IEEE Microw. Wireless Compon. Lett.*, vol. 26, no. 4, pp. 240–242, Apr. 2016.

[12] W. Chen, G. Zhang, S. Liu, and J. Yang, "Synthesis of multi-port filtering power divider for mixed topology using matrix optimization," *IEEE Trans. Circuits Syst. II, Exp. Briefs*, vol. 68, no. 1, pp. 176–180, Jan. 2021.

[13] S. Amari and G. Macchiarella, "Synthesis of inline filters with arbitrarily placed attenuation poles by using nonresonating nodes," *IEEE Trans. Microw. Theory Techn.*, vol. 53, no. 10, pp. 3075–3081, Oct. 2005.

[14] Y. Yang, M. Yu, and Q. Wu, "Advanced synthesis technique for unified extracted pole filters," *IEEE Trans. Microw. Theory Techn.*, vol. 64, no. 12, pp. 4463–4472, Dec. 2016.

[15] D. J. Simpson, R. Gómez-García, and D. Psychogiou, "Single-/multi-band bandpass filters and duplexers with fully reconfigurable transfer-function characteristics," *IEEE Trans. Microw. Theory Techn.*, vol. 67, no. 5, pp. 1854–1869, May 2019.

[16] X. Chen, W. Hong, Z. Hao, and K. Wu, "Substrate integrated waveguide quasi-elliptic filter using extracted-pole technique," in *Proc. Asia–Pacific Microw. Conf.*, Suzhou, China, Dec. 2005, pp. 556–558.

[17] G. Macchiarella, C. Tomasoni, E. Massoni, M. Bozzi, and L. Perregrini, "A novel class of half-mode SIW filters with extracted poles," in *Proc. 47th Eur. Microw. Conf.*, Madrid, Spain, Oct. 2017, pp. 807–810.

[18] E. Massoni, N. Delmonte, G. Macchiarella, L. Perregrini, and M. Bozzi, "Half-mode SIW filters with resonant couplings implementing transmission zeros," in *IEEE MTT-S Int. Microw. Symp. Dig.*, Pennsylvania, PA, USA, Jun. 2018, pp. 701–703.

[19] Y. Zhu and Y. Dong, "UIR-loaded dual-mode SIW filter with compact size and controllable transmission zeros," in *IEEE MTT-S Int. Microw. Symp. Dig.*, Los Angeles, CA, USA, Aug. 2020, pp. 667–670.

[20] R. J. Cameron, C. M. Kudsia, and R. R. Mansour, *Microwave Filters for Communication Systems: Fundamentals, Design, and Applications*. Hoboken, NJ, USA: Wiley, 2018.